Meccanica (2017) 52:1797–1808
DOI 10.1007/s11012-016-0543-7

The PELskin project—part III: a homogenized model of flows over and through dense poroelastic media

Giuseppe A. Zampogna · Alessandro Bottaro

Received: 2 March 2016 / Accepted: 16 September 2016 / Published online: 3 October 2016

Abstract In the context of the PELskin project, a homogenized model to study flows over and inside poroelastic media has been developed. It allows to simulate the fluid–structure interaction between a fluid and an extremely dense poroelastic medium, without limitations on physical and geometrical parameters such as the density of the elastic material, the porosity or the number of periodic microstructures which constitute the medium. The model is applied to the case of the flow in a channel driven by an oscillating pressure gradient, with half the channel covered by a carpet of flexible, densely packed fibers, connected to each other to allow for the propagation of the deformation field.

Keywords Poroelasticity · Homogenization

1 Introduction

Several phenomena are present in nature on the interaction between fluids and poroelastic materials. Studies both in hydrodynamics [1–3] and aerodynamics [4] have shown that the macroscopic motion of bodies coated by poroelastic microscopic structures is sensitively affected by the properties of the coating. Starting from this point, an European cooperation between the University of Aix-Marseille, the University of Manchester, the University of Freiberg, Wolf Dynamics s.r.l and The City University of London, has been formed with the ultimate goal of developing theoretical (the present work), numerical (cf. [5, 6]) and experimental (cf. [5, 6]) tools to better understand the physical mechanisms behind this kind of fluid–structure interaction. The modeling of these phenomena and, in particular, the behavior of poroelastic media can be implemented in different ways. Many of them presents theoretical or numerical limitations.

A microscopic pointwise approach which consists in performing direct numerical simulations using the Navier–Stokes equations in the interstitial zones between the pores and the equations of linear elasticity in the solid is very time-consuming in computational terms, but yields, in principle, the accurate behavior of the fluid and solid fields at the pore scale. Alternative techniques based on the *Immersed Boundary Method* (IBM) are less expensive and allow to understand what happens within the pores [6, 7], but have limitations on the geometrical configuration of the material (porosity and density of the solid skeleton per unit volume) and on the numerical treatment of limit cases (such as in the case of structures which, after large deformations, touch one another). A third category of applicable

G. A. Zampogna (✉) · A. Bottaro
DICCA, Università di Genova, Via Montallegro 1, 16145 Genoa, Italy
e-mail: giuseppe.zampogna@edu.unige.it

A. Bottaro
e-mail: alessandro.bottaro@unige.it

techniques is that of the fully macroscopic approaches where certain laws (such as Darcy's law in the case of rigid porous media) which model the global behavior of a homogenized medium, are assumed to be valid. These latter kinds of methods are computationally cheaper, but do not allow to analyze the flow at the pore scale [8].

The approach pursued here is a mixed microscopic–macroscopic one: adopting an upscaling procedure, we analyze the phenomenon at two levels. The lower level consists in deducing some microscopic physical properties of a poroelastic medium such as the permeability, the "effective" elasticity, the "bulk compliance of the solid skeleton" and the "effective fluid volume fraction" [9]. All of these quantities are to be intended not only as properties of a homogeneous continuum, which is a mixture of the elastic material and the fluid, but also of the type of flow and regime. The upper level consists in solving the governing (macroscopic) equations for the homogeneous material which can be written in closed form only if the unknowns in the lower level are already determined. Works which have already used this kind of approach [9, 10], determine the unknowns at the lower level using closure relations which are based on model microscopic problems. In the present work, instead, the differential problems at both levels are formally derived using homogenization on the basis of the theory outlined by Mei and Auriault [11], generalizing the procedure used for rigid porous media by Zampogna and Bottaro [16]: no closure problems are needed and the method is self-consistent for unbounded poroelastic media. The resulting model is computationally light and allows to treat arbitrary geometries without limitations on the porosity or others geometrical parameters (provided that the microscopic geometry is connected along every direction to allow for the propagation of the deformation field). The present approach complements other models, such as pointwise and IBM-based simulations, essentially for two reasons: the computational costs and the capability to treat very dense and flexible poroelastic materials.

In [11] and, in general, in the works which use homogenization, a treatment of heterogeneities cannot be found: the physical configurations solved are related to unbounded homogeneous regions with no need to dwell with boundary problems. Much effort has been devoted in the case of rigid porous media [12–17] to understanding if it is possible to use homogenization when its fundamental hypotheses (e.g. the assumption of microscopic periodicity) decay: the answer seems to be positive. The present work presents preliminary results for the interaction of a poroelastic medium in contact with a pure fluid region. A problem which does not arises when pointwise methods are used is the treatment of the macroscopic interface. Since the poroelastic medium is very dense, a macroscopic interface is created at the boundaries with the fluid region; such an interface can be viewed as a permeable membrane and must be modeled appropriately (see, e.g., Gopinath and Mahadevan [10]). Concerning the interface conditions for elastic media, one difficulty consists in the motion of the macroscopic interface. This difficulty is often avoided by imposing interface conditions at a fixed interface (usually identified with the initial resting state of the medium), assuming that the deformations are small or, equivalently, that the phenomenon is observed from a macroscopic point of view. The usual choice of the conditions to be imposed at the fixed interface is the continuity of the effective velocities and of the effective normal stresses [10, 18–20]. Thanks to a homogenized-based treatment of the H-medium, poroelastic phenomena which in the past could not be analyzed due to computational limitations, can now studied with applications in aerodynamics, aeroacoustic and hydrodynamic (cf. [1–4]), even beyond the objective of the PELskin project.

The paper is organized in three parts: after a briefly introduction to the homogenized-based model, the results are presented distinguishing between the solutions of the microscopic and macroscopic equations. The macroscopic problem treated is the motion of a fluid in an oscillating channel, covered, on one wall, by a thick carpet of flexible fibers. The oscillations of the carpet are analyzed and discussed in details.

2 Set up of the problem

Let us consider the oscillating flow of a Newtonian fluid with constant density ρ_f and viscosity μ in the plane channel sketched in Fig. 1. The flow is forced by an oscillating pressure gradient along the horizontal direction $\mathbf{e}_1$,

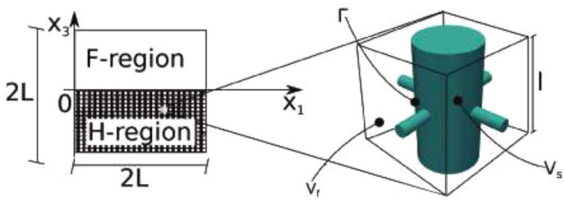

Fig. 1 Configuration of the problem, no-slip and periodic conditions are imposed on the *top* and *vertical* boundaries of the fluid domain in the *F*-region, respectively. A *zoom* inside the homogenized, poroelastic *H*-region highlights the microscopic fibrous structure which constitutes the poroelastic medium. V_f and V_s are the fluid and solid volumes inside the elementary cell, $V = V_s \cup V_f$, Γ is the fluid–structure interface

$$\nabla p = A\Re(\mathrm{e}^{\mathrm{i}\omega t})\mathbf{e}, \tag{1}$$

where A is the real amplitude of the wave, ω its frequency and $\Re$ denotes the real part. The channel is filled over half of its height (L) by a porous medium whose microscopic structure is shown in Fig. 1. In the fluid F-region and in the fluid portions V_f of the H-region, the Navier–Stokes equations (NSE) are valid. In the former region the NSE are rendered non-dimensional using P_F and l_F as pressure and length scales:

$$P_F = \rho_f U^2 \quad \text{and} \quad l_F = L, \tag{2}$$

where U is the velocity scale. The resulting NSE are

$$\dot{\mathbf{u}} + (\mathbf{u}\cdot\nabla)\mathbf{u} = \nabla\cdot\boldsymbol{\sigma}_F \quad \text{and} \quad \nabla\cdot\mathbf{u} = 0, \tag{3}$$

with $\boldsymbol{\sigma}_F = -p\mathbf{I} + 2\mathrm{Re}_L{}^{-1}\boldsymbol{\varepsilon}(\mathbf{u})$ and Re_L is the macroscopic Reynolds number, defined as $\mathrm{Re}_L = \rho_f UL/\mu$. The dependent variables $\mathbf{u}$ and p denote the velocity and static pressure fields. A dot over a variable's name denotes time differentiation; the operator $\boldsymbol{\varepsilon}$ is defined as $\boldsymbol{\varepsilon}(\mathbf{w}) = \frac{1}{2}(\nabla\mathbf{w}^T + \nabla\mathbf{w})$.

In the H-region the non-dimensional NSE for the fluid in the pores are deduced assuming that macroscopic pressure forces are equilibrated by local viscous dissipation, i.e.

$$\frac{P_H}{L} = \mu\frac{U}{l^2}, \tag{4}$$

and $l_H = l$, with l the microscopic length scale (cf. Fig. 1). The resulting equations read

$$\dot{\mathbf{u}} + (\mathbf{u}\cdot\nabla)\mathbf{u} = \nabla\cdot\boldsymbol{\sigma}_H \quad \text{and} \quad \nabla\cdot\mathbf{u} = 0, \tag{5}$$

with $\boldsymbol{\sigma}_H = -\epsilon^{-1}\mathrm{Re}_l^{-1}p\mathbf{I} + 2\mathrm{Re}_l^{-1}\boldsymbol{\varepsilon}(\mathbf{u})$, where Re_l is the microscopic Reynolds number defined as $\mathrm{Re}_l = \rho_f Ul/\mu$ and ϵ is a small parameter, ratio of the microscale l to the macroscale L.

In the region occupied by the solid, where poroelastic elements of constant density ρ_s are present, the classical equation of linear elasticity holds. The microscopic elasticity tensor $\mathbf{C}$, associated to an isotropic material, is rendered dimensionless using E, the Young's modulus of the material. The following order of magnitude relations are assumed:

$$E\frac{Pl^2}{\mu L^2}T_s = P_H, \quad U = \frac{V}{T_s} \quad \text{and} \quad \frac{\rho_s}{T_s^2} = \frac{E}{L^2}, \tag{6}$$

where T_s is the solid time scale. The resulting non-dimensional equations are

$$\epsilon^2\ddot{\mathbf{v}} = \nabla\cdot\boldsymbol{\Sigma}, \tag{7}$$

where $\boldsymbol{\Sigma}$ is the solid stress tensor, $\boldsymbol{\Sigma} = \mathbf{C} : \boldsymbol{\varepsilon}(\mathbf{v})$, with $\boldsymbol{\varepsilon}(\mathbf{v})$ the strain tensor. The NSE and the equations of elasticity are linked by the continuity of velocities and normal stresses on the solid–fluid microscopic interface Γ, i.e.

$$\mathbf{u} = \dot{\mathbf{v}}, \tag{8}$$

$$\boldsymbol{\Sigma}\cdot\mathbf{n} = \boldsymbol{\sigma}_H\cdot\mathbf{n}, \tag{9}$$

where $\mathbf{n}$ is the unit normal vector always assumed to point towards the fluid.

As already mentioned in the introduction, we follow a homogenization, multiscale procedure to develop a set of equations which holds in the homogenized domain (H-region in Fig. 1). The resulting model, in case of Stokes flow inside the poroelastic region, at leading order [21, 22] is:

$$\begin{cases} (1-\vartheta)\ddot{\mathbf{v}} = \nabla\cdot[\mathcal{C} : \boldsymbol{\varepsilon}(\mathbf{v}) - \boldsymbol{\alpha}p], \\ \langle\nabla\cdot\boldsymbol{\eta}\rangle\dot{p} - \nabla\cdot\mathcal{K}\cdot\nabla p = \langle\nabla\cdot\boldsymbol{\chi}\rangle : \boldsymbol{\varepsilon}(\dot{\mathbf{v}}) - \vartheta\nabla\cdot\dot{\mathbf{v}}, \\ \langle\mathbf{u}\rangle - \vartheta\dot{\mathbf{v}} = -\mathcal{K}\cdot\nabla p, \end{cases} \tag{10}$$

where $\langle\cdot\rangle$ denotes the average over the microscopic unit cell V (cf. Fig. 1) defined as the weighted integral on the whole microscopic cell; ϑ is the porosity of the medium defined as V_f/V. In system (10) the quantities $\mathcal{K}$, $\boldsymbol{\chi}$, $\boldsymbol{\eta}$, $\mathcal{C}$ and $\boldsymbol{\alpha}$ are microscopic unknowns which can be derived by homogenization. $\mathcal{K} = \langle\mathbf{K}\rangle$ is the *effective* permeability tensor solution of

$$\begin{cases} \nabla \mathbf{A} - \nabla^2 \mathbf{K} = \mathbf{I}, \\ \nabla \cdot \mathbf{K} = 0, \end{cases} \tag{11}$$

over V_f, plus V-periodicity. The unknown vector $\mathbf{A}$ which appears in the problem for $\mathbf{K}$ arises from homogenization, but is not used in the governing macroscopic equations.

The quantities $\boldsymbol{\chi}$ and $\boldsymbol{\eta}$ allow to define the *effective* elasticity tensor $\mathcal{C}$ and the matrix $\boldsymbol{\alpha}$ via the following equations:

$$\mathcal{C} = \langle \mathbf{C} : \boldsymbol{\varepsilon}(\boldsymbol{\chi}) \rangle + \langle \mathbf{C} \rangle \quad \text{and} \quad \boldsymbol{\alpha} = \vartheta \mathbf{I} + \langle \mathbf{C} : \boldsymbol{\varepsilon}(\boldsymbol{\eta}) \rangle \tag{12}$$

and satisfy the problems

$$\begin{cases} \nabla \cdot \mathbf{C} : \boldsymbol{\varepsilon}(\boldsymbol{\chi}) = 0, \\ \mathbf{C} : \boldsymbol{\varepsilon}(\boldsymbol{\chi}) \cdot \mathbf{n} = -\mathbf{C} : (\mathbf{I} \times \mathbf{I}) \cdot \mathbf{n} \quad \text{on } \Gamma, \end{cases} \tag{13}$$

$$\begin{cases} \nabla \cdot \mathbf{C} : \boldsymbol{\varepsilon}(\boldsymbol{\eta}) = 0, \\ [\mathbf{C} : \boldsymbol{\varepsilon}(\boldsymbol{\eta})] \cdot \mathbf{n} = \mathbf{n} \quad \text{on } \Gamma, \end{cases} \tag{14}$$

defined over V_s, plus V-periodicity. Once systems (11), (13) and (14) are solved, and the averaged quantities are computed, system (10) can be solved.

Using the domain decomposition technique, the solution in the F-region is coupled with the solution in the H-region using the following conditions imposed at the interface, $x_3 = 0$:

$$\langle \mathbf{u} \rangle|_H = \mathbf{u}|_F, \tag{15}$$

$$\langle \boldsymbol{\Sigma} \rangle \cdot \mathbf{n} = -\boldsymbol{\sigma}_F \cdot \mathbf{n}. \tag{16}$$

Furthermore, the condition:

$$(\mathbf{n} \cdot \mathcal{K}) \cdot \nabla p|_H = \frac{\mathcal{K}_f}{d_f} P^*|_{F-H}, \tag{17}$$

proposed by Gopinath and Mahadevan [10] is used to express the pressure jump through the interface, imagined to behave as a semipermeable thin membrane of thickness d_f and isotropic permeability $\mathcal{K}_f$, with $P^*|_{F-H}$ the pressure difference across the skin. The ratio $\mathcal{K}_f/d_f$ is a priori unknown and must be tuned for each configuration of the flow.

3 Microscopic results

As already noted, the microscopic variables are V-periodic. The chosen geometry (shown in Fig. 1) consists of cylinders, with longitudinal axis normal to the surface to which they are hinged, linked to one another by thin transversal cylinders. The lattice formed allows the cylinders to interact avoiding problems related to the microperiodicity assumption [19, 21]. Starting from a simple vertical cylinder, Table 1 shows how the porosity changes by varying the ratio d_t/d, where d_t is the diameter of the transversal connecting cylinders and d that of the main fiber aligned along x_3. All the solvers for the microscopic problems are based on OpenFoam: time-marching solvers, with the Euler scheme, are used to solve problems (11, 13, 14). We refer to [21] for further details about numerical tests and schemes.

Table 1 Behavior of the porosity as function of the ratio d_t/d for a porosity ϑ in the vicinity of 0.8

Main cyl.	$d/d_t = 7.5$	$d/d_t = 5$	$d/d_t = 2.5$	$d/d_t = 1$
$\vartheta = 0.8$	$\vartheta = 0.797$	$\vartheta = 0.793$	$\vartheta = 0.768$	$\vartheta = 0.583$
$r = 0.252$	$r_t = 0.034$	$r_t = 0.050$	$r_t = 0.101$	$r_t = 0.252$

3.1 The permeability tensor $\mathcal{K}_{ij}$

The solution of problem (11) has already been described in [16], we limit here only to showing how the permeability changes by varying the ratio d/d_t for some chosen physical parameters. We observe that even if ϑ varies only by about 4 % (except in the limit case of $d/d_t = 1$) with respect to the reference value of $\vartheta = 0.8$ of the unconnected case, for which $d_t = 0$, the changes in the permeability are rather relevant. The values assumed by the effective permeability are shown in Table 2 for the Stokes flow case. The fact that the permeability tensor changes much even if the porosity does not, is desirable because it is an indication that the information related to the structure passed to the macroscopic equations is not a simple function of porosity. The permeability decreases monotonically when the porosity is reduced, i.e. when the ratio d/d_t decreases; for all cases analyzed the structure is cubic symmetric and this is confirmed also by the form of $\mathcal{K}_{ij}$.

3.2 The effective elasticity tensor $\mathcal{C}_{ijpq}$

In order for definition (12) and equations (13) and (14) to make sense we introduce the microscopic elasticity

Table 2 Values of the non-zero components of the tensor $\mathcal{K}$ for varying the ratio d/d_t and $\vartheta \approx 0.8$

	$\mathcal{K}_{11} = \mathcal{K}_{22}$	$\mathcal{K}_{33}$
$d = d_t$	9.4×10^{-5}	9.4×10^{-5}
$d = 2.5d_t$	2.0×10^{-4}	4.1×10^{-4}
$d = 5d_t$	2.5×10^{-4}	4.7×10^{-4}
$d = 7.5d_t$	5.2×10^{-3}	1.1×10^{-2}
$d_t = 0$	1.9×10^{-2}	3.9×10^{-2}

The case $d_t = 0$ corresponds to disconnected fibers aligned with x_3, for Re $= \mathcal{O}(\epsilon)$

tensor C_{ijkl}, expressed as a 6×6 matrix in Voigt's contracted notation [23]. If we consider an isotropic elastic material, C_{ijkl} assumes the following form:

$$C_{ijkl} = \begin{pmatrix} \lambda+2\mu & \lambda & \lambda & 0 & 0 & 0 \\ \lambda & \lambda+2\mu & \lambda & 0 & 0 & 0 \\ \lambda & \lambda & \lambda+2\mu & 0 & 0 & 0 \\ 0 & 0 & 0 & \mu & 0 & 0 \\ 0 & 0 & 0 & 0 & \mu & 0 \\ 0 & 0 & 0 & 0 & 0 & \mu \end{pmatrix} \tag{18}$$

where λ and μ are the Lamé constants of the isotropic material, normalized by Young's modulus of elasticity. In terms of Poisson's ratio ν_P, the following relations hold:

$$\lambda = \frac{\nu_P}{(1+\nu_P)(1-2\nu_P)} \quad \text{and} \quad \mu = \frac{1}{2(1+\nu_P)}. \tag{19}$$

We consider here a soft ($E = 3 \times 10^{-4}$ GPa) polyurethane foam with $\nu_P = 0.40$, that is $\lambda = 1.42, \mu = 0.36$. The tensor χ_i^{pq} in system (13) represents a microscopic displacement; such a system is formed by linear PDE's obtained as a combination of the entries of the pointwise elasticity tensor C_{ijkl} and of the jacobian of χ_i^{pq}, valid over the solid structure inside the microcell. In Fig. 2 an example of the microscopic fields is shown. Several symmetries can be observed also at a macroscopic level in the *effective* stiffness tensor ($\mathcal{C}_{1111} = \mathcal{C}_{2222}$, $\mathcal{C}_{1122} = \mathcal{C}_{2211}$, $\mathcal{C}_{1313} = \mathcal{C}_{2323}$ and $\mathcal{C}_{1133} = \mathcal{C}_{2233} = \mathcal{C}_{3322} = \mathcal{C}_{3311}$), so that the tensor has the form:

$$\mathcal{C}_{ijkl} = \begin{pmatrix} \bigcirc & \blacksquare & \otimes & 0 & 0 & 0 \\ \blacksquare & \bigcirc & \otimes & 0 & 0 & 0 \\ \otimes & \otimes & \bigstar & 0 & 0 & 0 \\ 0 & 0 & 0 & \clubsuit & 0 & 0 \\ 0 & 0 & 0 & 0 & \clubsuit & 0 \\ 0 & 0 & 0 & 0 & 0 & \spadesuit \end{pmatrix}, \tag{20}$$

in agreement with [24, 25]; in particular, the specific values computed for the linked cylinders geometry are shown in Table 3. As one can observe, the structure realized with $d = d_t$ shows cubic symmetries (i.e. there are 9 planes of symmetry) and the structure of $\mathcal{C}_{ijkl}$ agrees with the theory of solid mechanics [25]. For the case $d = 2.5d_t$ the presence of the transverse cylinders is important, and this can be seen in the effective stiffness tensor which also in this case shows cubic symmetries; information about the transverse isotropy of the principal cylinder is maintained as it can be inferred observing that $\mathcal{C}_{1212} \neq \mathcal{C}_{1313} = \mathcal{C}_{2323}$. Increasing the ratio d/d_t, $\mathcal{C}_{ijkl}$ approaches the tensor computed for the case of disconnected cylinders ($d_t = 0$). A further confirmation of the fact that the elasticity tensor has a physical behavior is done by a parametric study for varying ϑ. For $\vartheta \to 0$ we recover, in facts, the values of the pointwise elasticity tensor $\mathbf{C}$.

The parametric study conducted demonstrates that a range of porosities exists for which the shear modulus is negative. Whereas this might appear strange at first sight, there is no theoretical law which establishes the

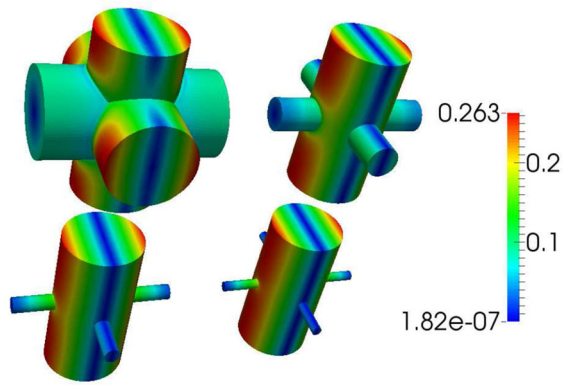

Fig. 2 Example of one vector field χ_i^{11}; magnitude for four different values of the ratio d/d_t: 1, 2.5, 5, 7.5

Table 3 Values of $\mathcal{C}_{ijpq}$, for varying the ratio d/d_t and $\vartheta \approx 0.8$

	○	■	⊗
$d = d_t$	2.024×10^{-1}	2.862×10^{-2}	2.862×10^{-2}
$d = 2.5d_t$	4.928×10^{-2}	1.841×10^{-2}	8.767×10^{-2}
$d = 5d_t$	4.433×10^{-3}	1.061×10^{-3}	2.239×10^{-4}
$d = 7.5d_t$	4.687×10^{-4}	2.336×10^{-4}	1.648×10^{-4}
$d_t = 0$	0	0	0
	★	♠	♣
$d = d_t$	2.024×10^{-1}	-3.395×10^{-2}	-3.395×10^{-2}
$d = 2.5d_t$	2.688×10^{-1}	-6.658×10^{-3}	-1.067×10^{-2}
$d = 5d_t$	1.985×10^{-1}	-6.001×10^{-3}	-8.349×10^{-3}
$d = 7.5d_t$	2.613×10^{-1}	-4.629×10^{-3}	-2.307×10^{-3}
$d_t = 0$	2.055×10^{-1}	0	0

The case $d_t = 0$ corresponds to the simple (disconnected) cylinder geometry; in this case there is a single non-zero entry of the *effective* stiffness tensor (20) and there is no propagation of the displacement field [19, 21]

positive definiteness of the tensor. On the other hand, composite materials with negative shear modulus have been reported in the literature [26, 27].

4 Macroscopic solution

The macroscopic solver, written in Matlab, provides a solution of the NSE in the F-region written as in (3). Using the normalizations in (2) to scale the pressure and the displacement, the resulting macroscopic model valid in the H-region becomes:

$$\begin{cases} (1-\vartheta)\ddot{\mathbf{v}} = \epsilon^4 \left(\dfrac{\mathrm{Re}_L}{\mathrm{Ca}}\right)^2 \nabla \cdot [\mathcal{C} : \boldsymbol{\varepsilon}(\mathbf{v}) - \mathrm{Ca}\boldsymbol{\alpha} p], \\ \mathrm{Ca}\beta\dot{p} - \epsilon^2 \mathrm{Re}_L \nabla \cdot \mathcal{K} \cdot \nabla p = \langle \nabla \cdot \boldsymbol{\chi} \rangle : \boldsymbol{\varepsilon}(\dot{\mathbf{v}}) - \vartheta \nabla \cdot \dot{\mathbf{v}}, \\ \langle \mathbf{u} \rangle - \vartheta \dot{\mathbf{v}} = -\epsilon^2 \mathrm{Re}_L \mathcal{K} \cdot \nabla p, \end{cases} \tag{21}$$

where Ca denotes the Cauchy number defined by $\mathrm{Ca} = \rho\omega^2 L^2/E$ and $\beta = \langle \nabla \cdot \boldsymbol{\eta} \rangle$ is the *bulk compliance* of the solid skeleton. The interface conditions (15) and (17) remain unchanged while equation (16) becomes

$$-\mathrm{Ca}\, p\, \mathbf{n} + 2\frac{\mathrm{Ca}}{\mathrm{Re}_L} \boldsymbol{\varepsilon}(\mathbf{u}) \cdot \mathbf{n} = \mathcal{C} : \boldsymbol{\varepsilon}(\mathbf{v}) \cdot \mathbf{n}. \tag{22}$$

Since a study of the numerics is out of scope of the paper we refer to [21] for further details on this.

4.1 Fluid simulation without poroelastic medium

A Navier–Stokes solver has been developed using the fractional step method in order to decouple pressure and velocity. The spatial operators have been discretized using fourth-order finite differences and the Adam–Bashfort schemes is adopted for the time integration. In order to validate the code, a fluid simulation has been performed in a 2×2 channel with periodic inlet–outlet and no-slip conditions at the lower and upper walls. The pressure gradient reads as in equation (1) where $A = \omega = 1$ and $\mathrm{Re}_L = 100$. The fluid solver has been validated using the analytical solution [28]. In Fig. 3 the velocity profiles of the analytical and numerical solution, for a fixed x_1 are represented at different instants in a cycle. The comparison shows a good match between the two solutions.

4.2 Test cases for the behavior of a poroelastic layer

A second solver has been developed in order to solve the homogenized equations (21), based on the same numerical schemes to integrate in space and time. To ensure that the homogeneous model simulates the behavior of a linear elastic solid, we propose here two simplified tests. In the first case we neglect the fluid flow, solving only the first equation of system (21) without the pressure contribution. An infinitely long and wide layer of thickness L is considered. At

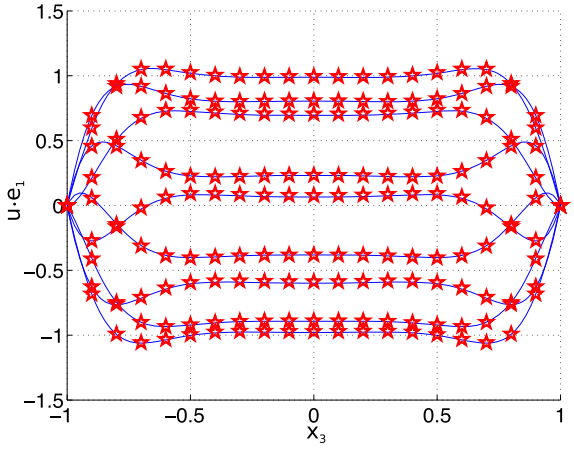

Fig. 3 Horizontal velocity profiles for $x_1 = 1$ at different instants during a cycle. *Symbols star* represent the analytical solution and the *solid lines* the numerical ones

$x_3 = -1$, zero displacement is imposed, while on the top ($x_3 = 0$) constant shear and zero normal stresses are enforced. In this case $\mathrm{Re}_L = 100$, $\mathrm{Ca} = 9.15 \times 10^{-8}$ and $\epsilon = 4 \times 10^{-5}$. The simulation is performed with the values of $\mathcal{C}$ for $d = 2.5 d_t$ in Table 3. With these boundary conditions we find a steady solution which represents the behavior of a linear elastic material: the horizontal displacement, constant along x_1, has a linear distribution along x_3, and the vertical displacement is zero (Fig. 4).

In the second case we solve also for the fluid pressure field (i.e. we consider the first two equations of system (21)): the pressure is supposed to be linear at the top of the poroelastic layer ($x_3 = 0$) and a homogeneous Neumann condition is imposed at $x_3 = -1$ (to guarantee no-penetration of the fluid). Since we want to simulate an infinitely long layer, periodic pressure gradient is imposed at the vertical boundaries of the computational domain in order to maintain the periodicity of the effective velocities [which can be recovered a posteriori using the third equation of system (21)]. Also in this case we obtain a steady solution shown in Fig. 5: the horizontal displacement is the same of the previous case, while a non-zero vertical displacement arises from the boundary condition (which includes the pressure) imposed at the top of the layer for $\mathbf{v} \cdot \mathbf{e}_3$. The horizontal effective velocity $(\langle \mathbf{u} \rangle - \vartheta \dot{v}) \cdot \mathbf{e}_1$ is constant, equal to $-\epsilon \mathrm{Re}_l \mathcal{K}_{33} \nabla p \cdot \mathbf{e}_1|_{x_3=0} = -0.5213$ and the vertical effective velocity is zero. Since the third equation of system (21), in the steady case, reduces to Darcy's law, we reproduce the same solution obtained with the model described in [16], an indication of the fact that the model, for this

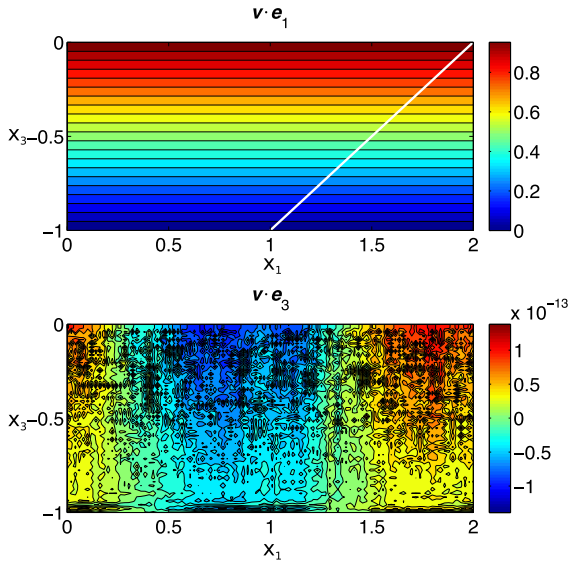

Fig. 4 Horizontal and vertical displacement for the first test case described in Sect. 4.2

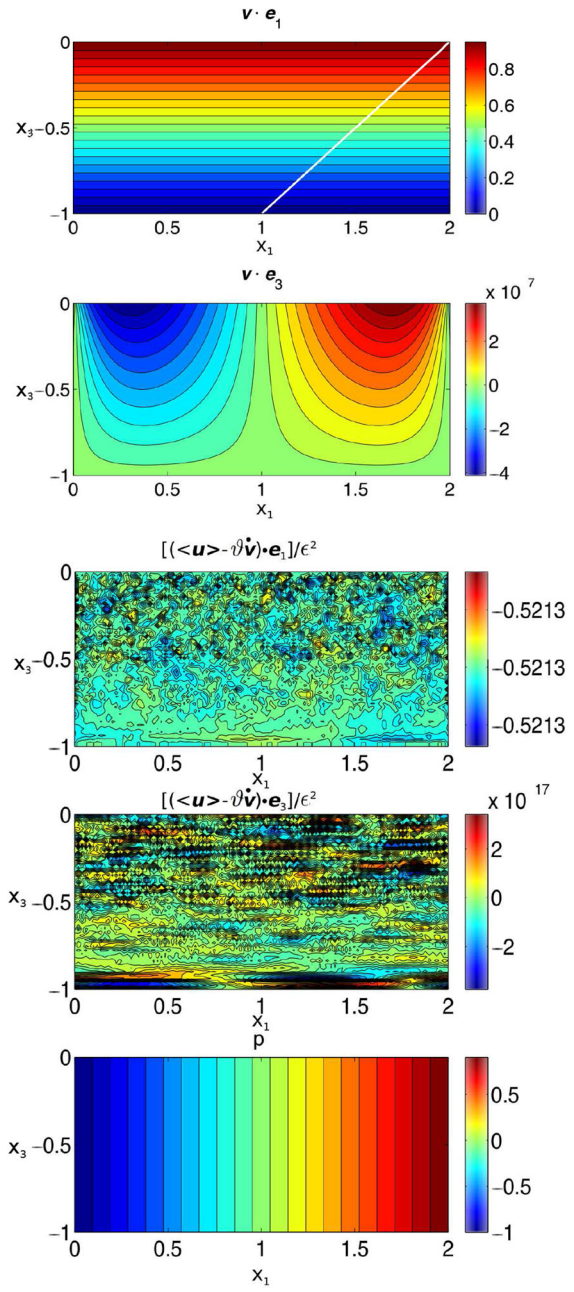

Fig. 5 From *top* to *bottom* horizontal and vertical displacement, horizontal and vertical effective velocity and pressure for the second test case described in Sect. 4.2

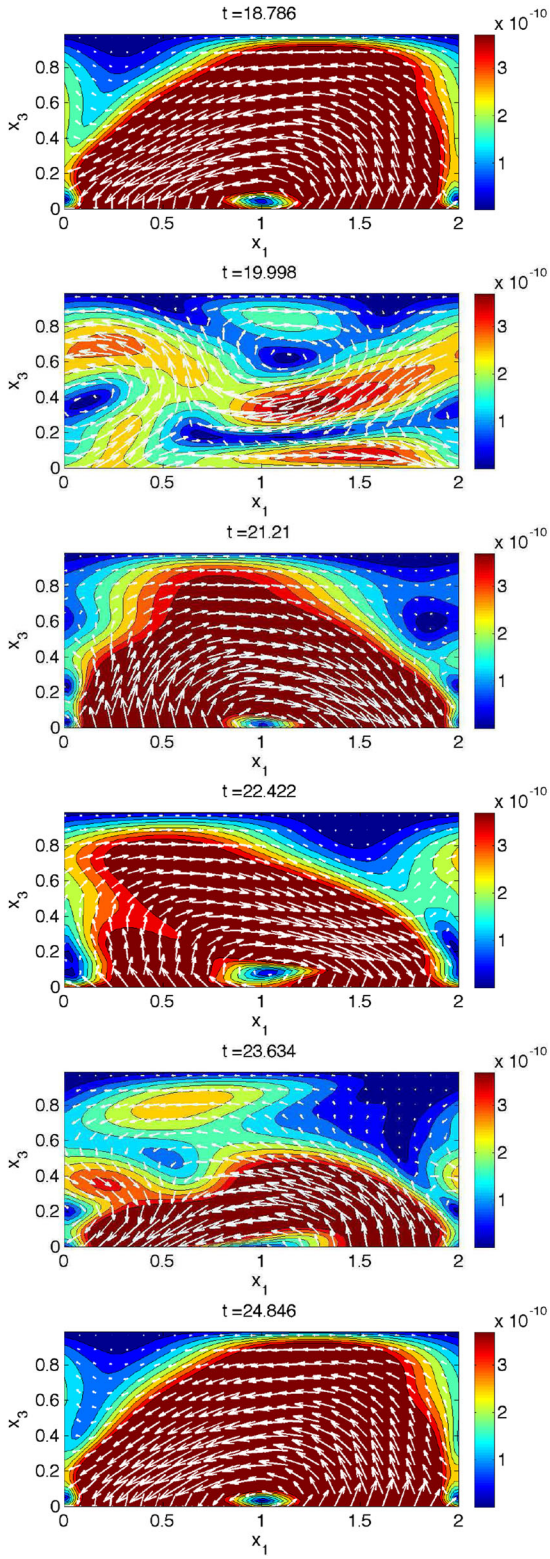

◀**Fig. 6** Disturbance velocity field $\tilde{\mathbf{u}}$ in the F-region at six different instants during the periodic cycle. The *contours* represent the local kinetic energy of the disturbance field and the arrows its velocity

steady case, is reliable. At this point, we can move to an unsteady configuration.

4.3 Two-way simulation with poroelastic medium

The solvers introduced in Sects. 4.1 and 4.2 have been coupled to solve a case in which a homogeneous poroelastic medium fills the lower half of the channel (cf. Fig. 1). As already done in the second test case, the first two equations of system (21) are solved in the H-region and the velocity is recovered a posteriori from the displacement and pressure fields (i.e. from the modified Darcy's law). For this reason, only boundary conditions for displacement and pressure are needed. The two solvers are coupled with a domain decomposition technique to find the solution in the mixed domain (F plus H-regions). We refer to [29] where it is shown that the method used is suitable also for unsteady problems. This technique consists in solving for the pure-fluid and the homogeneous material iteratively. Conditions (15, 17, 22) are used at the boundary between F and H—the interface—to transfer information: equation (15) from the poroelastic region to the fluid region and equations (17, 22) in the opposite sense.

Also with this configuration, in order to allow for periodicity along x_1, periodic conditions are imposed for the displacement and for the pressure gradient at the vertical boundaries of H. The simulation shown here is done for the following conditions: the fluid is air ($\nu = 1.55 \times 10^{-5}\mathrm{m}^2/\mathrm{s}$), $\mathrm{Re}_L = 100$ and the material is a very soft and dense polyurethane foam with a microscopic structure organized as in Fig. 2 with $d/d_t = 2.5$. With these values $\mathrm{Ca} = 9.15 \times 10^{-8}$. The parameter ϵ is chosen equal to 4×10^{-5}, which, in other words, means that the microstructure is repeated about 2.5×10^4 times per unit length. The parameter K_f and d_f are such that $K_f = \epsilon \mathrm{Re}_l \mathcal{K}_{33}$ and $d_f = \epsilon$: since the thickness of the membrane has been chosen equal to the height of one elementary cell, the membrane's permeability can be assumed equal to the vertical component of $\mathcal{K}$. As before, the oscillating pressure

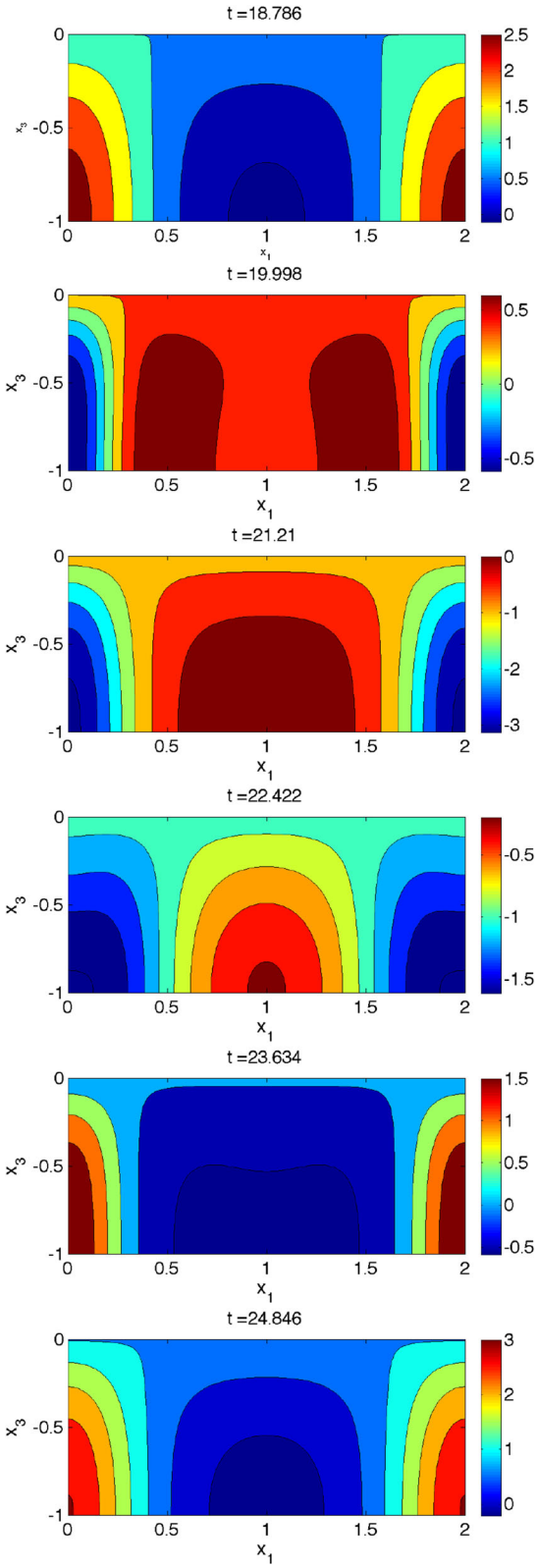

◀**Fig. 7** Horizontal component of the effective velocity field $((\mathbf{u}^* - \vartheta\dot{\mathbf{v}})/\epsilon^2)$ in the *H*-region at six different instants during the periodic cycle

gradient is characterized by non-dimensional amplitude and frequency equal to 1.

The new fluid velocity in the *F*-region can be written as

$$\mathbf{u}^* = \mathbf{u} + \tilde{\mathbf{u}}, \tag{23}$$

where $\mathbf{u}$ is the solution computed imposing an impermeable wall at $x_3 = 0$ and $\tilde{\mathbf{u}}$ is the disturbance due to the effect of the poroelastic medium. The amplitude of such disturbances has the same order of magnitude of the effective velocity in the *H*-region defined as $\mathbf{u}^* - \vartheta\dot{\mathbf{v}}$, i.e. about $\mathcal{O}(\epsilon \mathrm{Re}_l \mathcal{K})$. In Fig. 6 the fluid flow disturbances at different instants during the periodic cycle are represented. The contours represent the kinetic energy of $\tilde{\mathbf{u}}$, while the white arrows display the disturbance velocity field.

The effective fluid velocity field in the *H*-region is represented in Figs. 7 and 8, normalized by the constants $\epsilon \mathrm{Re}_l(\mathbf{e}_1 \cdot \mathcal{K} \cdot \mathbf{e}_1)$ and $\epsilon \mathrm{Re}_l(\mathbf{e}_3 \cdot \mathcal{K} \cdot \mathbf{e}_3)$ for the x_1 and x_3 components of the velocity, respectively.

The displacement of the poroelastic structure is represented in Figs. 9, 10 and 11. Figure 9 shows how the displacement changes in time, along x_3 and for a fixed x_1 in the channel. Figure 10 shows the correlation in time between the horizontal and vertical displacements. After one cycle the curves overlap and the motion of the structure is fully periodic. In Fig. 11 the vertical position of the macroscopic fluid–structure interface is represented: even if the interface conditions (15, 17, 22) have been imposed for a fixed $x_3 = 0$, thanks to the continuity of normal stresses, the procedure lets the interface move in the vertical direction of a distance smaller than ϵ.

5 Conclusions and outlook

An upscaling technique based on homogenization has been used to study the flow over and through a poroelastic medium coating one wall of a channel. The flow studied is forced by an oscillating pressure gradient. A general strategy suitable for every kind of micro-periodically connected geometry and, in

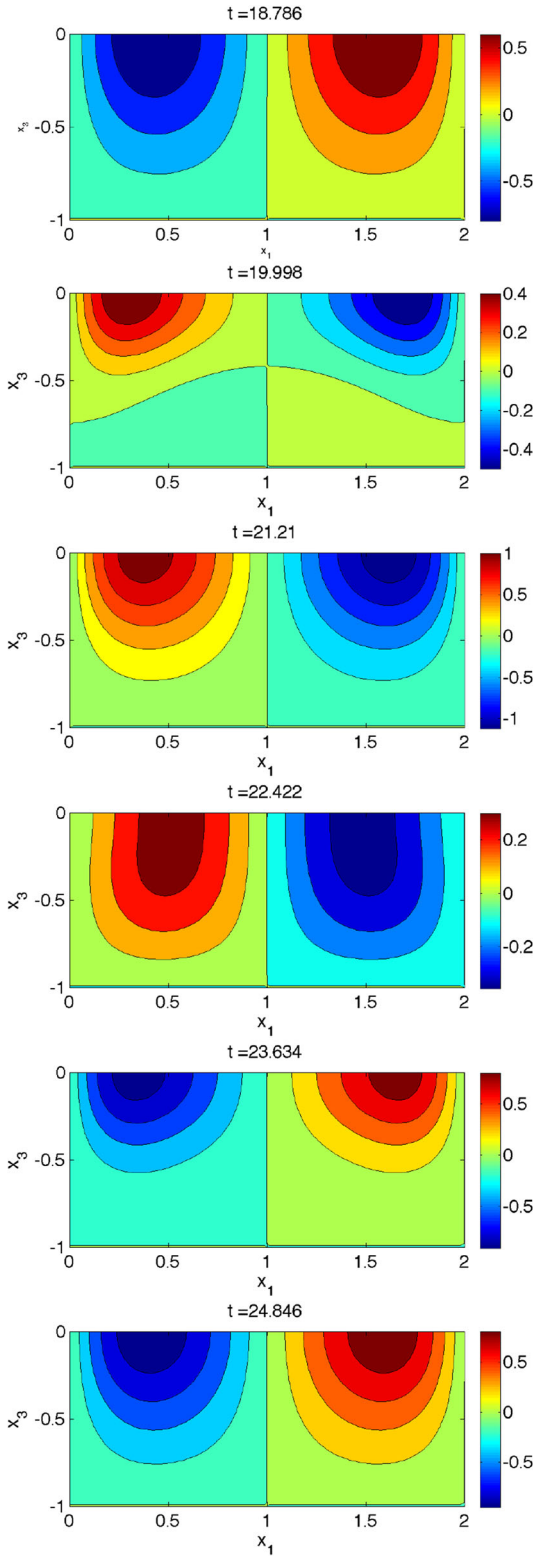

◀**Fig. 8** Vertical component of the effective velocity field $((\mathbf{u}^* - \vartheta\dot{\mathbf{v}})/\epsilon^2)$ in the H-region at six different instants during the periodic cycle

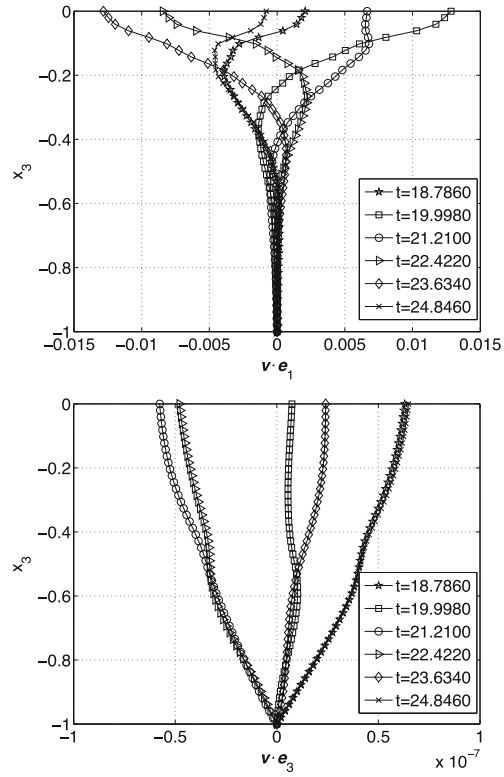

Fig. 9 Horizontal (*upper frame*) and vertical (*lower frame*) displacement along x_3 for $x_1 = 1.5$ in the channel at six different instants during the period

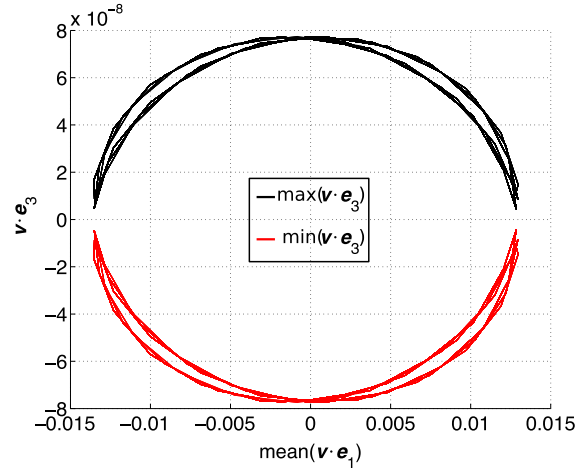

Fig. 10 Mean horizontal displacement of the interface of the homogenized structure versus maximum and minimum vertical displacement

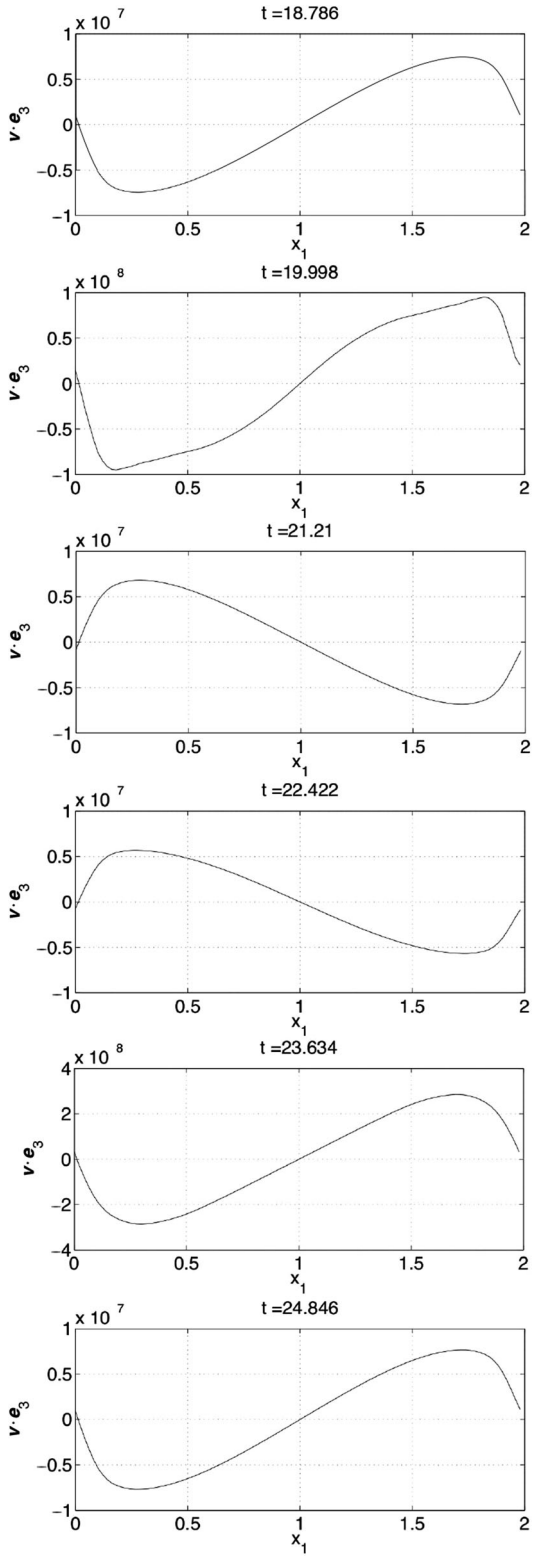

◀**Fig. 11** Vertical displacement of the interface for six different instants within a period

particular, for bio-inspired structures has been used. The work has been developed from two points of view: the microscopic and the macroscopic one. The microscopic equations provide a characterization of the particular geometry of the porous medium, resulting in an estimate for the components of the permeability and the *effective* elasticity tensors, in agreement with previous results. From a macroscopic point of view a solver for the present configuration has been developed and validated, in the free-fluid region, on the basis of the results present in the literature. The particular microscopic structure used and the high density of the poroelastic medium (i.e. the large number of microstructures per unit volume) render a comparison with other numerical results difficult. Qualitative observations can however be made:

- even if small, the displacement of the interface is not constant (both along the horizontal and the vertical direction) and the interface assumes a wavy configuration. This fact indicates that a *honami*-like effect can be simulated, laying the groundwork for new studies;
- different portions of the poroelastic continuum positioned in different parts of the domain do not oscillate in phase when subject to harmonic volume forcing. This means that a real elastic behavior of the structure can be encountered; despite the fact that homogenization is based on the hypothesis of microscopic periodicity, this does not bear onto the macroscopic behaviour.

Acknowledgments The financial support of the European Commission through the PELskin FP7 European project (AAT .2012.6.3-1. Breakthrough and emerging technologies) is gratefully acknowledged. We are thankful to the project's partners for several interesting discussions, and we also acknowledge fruitful interactions with S. Bagheri and U. Lacis.

References

1. Wen L, Weaver JC, Lauder GV (2014) Biomimetic shark skin: design, fabrication and hydrodynamic function. J Exp Biol 217:1656–1666

2. Ghisalberti M, Nepf HM (2006) The structure of the shear layer over rigid and flexible canopies. Environ Fluid Mech 6(3):277–301
3. Oeffner J, Lauder GV (2012) The hydrodynamic function of shark skin and two biomimetic applications. J Exp Biol 215:785–795
4. Jaworski JW, Peake N (2013) Aerodynamic noise from a poroelastic edge with implications for the silent flight of owls. J Fluid Mech 723:456–479
5. Pinelli A, Omidyeganeh M, Brücker C, Revell A, Sarkar A, Alinovi E (2016) The PELskin project—part IV: control of bluff bodies wakes using hairy filaments. Meccanica. doi:10.1007/s11012-016-0513-0
6. Li C, Favier J, Kamps L, Revell A, O'Connor J, Brücker C (2016) The PELskin project—part I: fluid-structure interaction for a row of flexible flaps: a reference study in oscillating channel flow. Meccanica. doi:10.1007/s11012-016-0521-0
7. Favier J, Revell A, Pinelli A (2014) A Lattice Boltzmann—immersed boundary method to simulate the fluid interaction with moving and slender flexible objects. J Comput Phys 261:145–161
8. Rice JR, Cleary MP (1976) Some basic stress diffusion solution for fluid-saturated elastic porous media with compressible costituents. Rev Gephys Space Phys 14:227–241
9. Skotheim JM, Mahadevan L (2003) Dynamics of poroelastic filaments. Proc R Soc Lond 460:1995–2020
10. Gopinath A, Mahadevan L (2011) Elastohydrodynamics of wet bristles, carpets and brushes. Proc R Soc 467(2130):1–21
11. Mei CC, Auriault JL (1991) The effect of weak inertia on flow through a porous medium. J Fluid Mech 222:647–663
12. Ochoa-Tapia JA, Whitaker S (1995) Momentum transfer at the boundary between a porous medium and a homogeneous fluid I. Theoretical development. Int J Heat Mass Transf 38:2635–2646
13. Ochoa-Tapia JA, Whitaker S (1995) Momentum transfer at the boundary between a porous medium and a homogeneous fluid II. Comparison with experiment. Int J Heat Mass Transf 38:2647–2655
14. Ochoa-Tapia JA, Whitaker S (1998) Momentum jump condition at the boundary between a porous medium and a homogeneous fluid: inertial effects. J Porous Media 1:201–217
15. Le Bars M, Worster M (2006) Interfacial conditions between a pure fluid and a porous medium: implications for binary alloy solidification. J Fluid Mech 550:149–173
16. Zampogna GA, Bottaro A (2016) Fluid flow over and through a regular bundle of rigid fibres. J Fluid Mech 792:5–35
17. Lācis U, Bagheri S (2016) A framework for computing effective boundary conditions at the interface between free fluid and a porous medium. arXiv:1604.02880v2
18. Barry SI, Parker KH, Aldis GK (1991) Fluid flow over a thin deformable porous layer. J Appl Math Phys 42:633–647
19. Hoffmann KH, Botkin ND, Starovoitov VN (2004) Homogenization of interfaces between rapidly oscillating fine elastic structures and fluids. SIAM J Appl Math 65(3):983–1005
20. Alexiou TS, Kapellos GE (2013) Plane Couette-Poiseuille flow past a homogeneous poroelastic layer. Phys fluid 25(073605):1–17
21. Zampogna GA (2016) Homogenized-based modeling of flows over and through poroelastic media. Ph.D thesis, Univ. of Genova, Italy
22. Mei CC, Vernescu B (2010) Homogenization methods for multiscale mechanics. World Scientific, Singapore
23. Voigt W (1889) Ueber die beziehung zwischen den beiden elasticitätsconstanten isotroper körper. Ann Phys 274(12):573–587
24. Cheng AHD (1997) Material coefficients of anisotropic poroelasticity. Int J Rock Mech 34(2):199–205
25. Cowin SC (2013) Continuum mechanics of anisotropic materials. Springer, New York
26. Lakes RS, Lee T, Bersie A, Wang YC (2001) Extreme damping in composite materials with negative-stiffness inclusions. Nature 410:565–567
27. Wu Y, Lai Y, Zhang ZQ (2011) Elastic metamaterials with simultaneously negative effective shear modulus and mass density. Phys Rev Lett 107:105506
28. Landau LD, Lifshitz EM (1959) Fluid mechanics. U.S.S.R. Academy of Science, Pergamon Press, Oxford
29. Quarteroni A, Valli A (1999) Domain decomposition methods for partial differential equations. Oxford University Press, Oxford